Molecular Therapy
Nucleic Acids
Original Article

Long Noncoding RNA *lnc-HC* Regulates PPARγ-Mediated Hepatic Lipid Metabolism through *miR-130b-3p*

Xi Lan,[1,2] Litao Wu,[1,2] Nan Wu,[1,2] Qian Chen,[1,2] Yue Li,[1,2] Xiaojuan Du,[1,2] Chenxi Wei,[1,2] Lina Feng,[1,2] Yazhao Li,[1,2] Ezra Kombo Osoro,[1,2] Mengyao Sun,[1,2] Qilan Ning,[1,2] Xiaofei Yan,[1,2] Xudong Yang,[1,2] Dongmin Li,[1,2] and Shemin Lu[1,2]

[1]Department of Biochemistry and Molecular Biology, School of Basic Medical Sciences, Xi'an Jiaotong University Health Science Center, Xi'an, Shaanxi 710061, China; [2]Key Laboratory of Environment and Genes Related to Diseases (Xi'an Jiaotong University), Ministry of Education of China, Beijing, China

Nonalcoholic fatty liver disease (NAFLD) is due to the excessive lipid accumulation within hepatocytes. Metabolic nuclear receptors (MNRs) play great roles in lipid homeostasis. We have identified a novel long noncoding RNA (lncRNA), *lnc-HC*, which regulates hepatocytic cholesterol metabolism through reducing *Cyp7a1* and *Abca1* expression. Here, we further elucidate its roles in hepatic fatty acid and triglyceride (TG) metabolism through a novel lncRNA regulatory mechanism. The most prominent target of *lnc-HC* identified by *in vitro* study is *PPARγ*. Further studies revealed that *lnc-HC* negatively regulates *PPARγ* at both the mRNA and protein levels and suppresses hepatocytic lipid droplet formation. Importantly, the function of *lnc-HC* in regulating *PPARγ* expression depends on modulating *miR-130b-3p* expression from the transcriptional to the post-transcriptional level, not through lncRNA's critical modulating patterns. *In vivo*, the reduction of *lnc-HC* expression significantly decreases *miR-130b-3p* expression, induces *PPARγ* expression, and increases TG concentration in rat livers with hyperlipidemia. These findings further help in understanding the regulatory pattern of lnc-HC in hepatic lipid metabolism and might present a possible therapeutic target for improving lipid homeostasis.

INTRODUCTION

Nonalcoholic fatty liver disease (NAFLD) is one type of fatty liver disease that occurs in liver as lipid accumulation and hepatic steatosis due to causes other than alcohol uptake. NAFLD ranges from nonalcoholic fatty liver to nonalcoholic steatohepatitis, hepatic fibrosis, and cirrhosis,[1,2] and can even become hepatic carcinoma.[3,4] Furthermore, NAFLD is also closely associated with type II diabetes, atherosclerosis, and cardiovascular disease.[4–6] Recent studies indicate that over 30% of people in the United States and up to 25% of adults worldwide have NAFLD.[7,8] Although a growing number of studies help us understand the pathogenesis of NAFLD, we still lack an approved therapeutic regime due to its complexity. Thus, exploring the pathological process of NAFLD and discovering the critical drug targets could greatly contribute to understanding the molecular mechanism and supplying promising therapeutic candidates.

NAFLD manifests hepatocellular lipid deposits and injury as the main pathological change, which is caused by lipid disorder. Metabolic nuclear receptors (MNRs), as a big class of transcription factors (TFs), are critical contributors to energy and lipid homeostasis. MNR family contains peroxisome-proliferator-activated receptors (PPARs), liver X-activated receptors (LXRs), and the farnesoid X receptor (FXR).[9,10] PPARs mainly participate in lipogenesis and insulin resistance. PPARγ powerfully regulates fatty acid uptake and storage and has been implicated in the pathology of obesity, diabetes, and atherosclerosis.[11,12] Although PPARγ is a well-known therapeutic target in the treatment of hyperlipidemia and hyperglycemia in type 2 diabetes, PPARγ agonist causes adverse events such as liver function disorder and weight gain.[13]

Existing studies have identified important roles for long noncoding RNAs (lncRNAs) in lipid metabolism.[14–17] Ectopic expression of the lncRNA HOTAIR in abdominal preadipocytes could upregulate adipogenic gene expression of PPARγ and lipoprotein lipase (LPL) and induce the adipocyte differentiation.[18] Blnc1 interacts with transcription factor EBF2 and promotes brown and beige adipocyte differentiation, which is linked to thermogenesis and systemic energy homeostasis.[19] The lncRNA lncLSTR regulates lipid homeostasis through TDP-43/FXR/apoC2 molecular pathways.[20]

Received 19 September 2019; accepted 16 October 2019;
https://doi.org/10.1016/j.omtn.2019.10.018.

Correspondence: Xi Lan, Department of Biochemistry and Molecular Biology, School of Basic Medical Sciences, Xi'an Jiaotong University Health Science Center, Xi'an, Shaanxi 710061, China.
E-mail: lanxi.2016@xjtu.edu.cn
Correspondence: Shemin Lu, Department of Biochemistry and Molecular Biology, School of Basic Medical Sciences, Xi'an Jiaotong University Health Science Center, Xi'an, Shaanxi 710061, China.
E-mail: lushemin@mail.xjtu.edu.cn

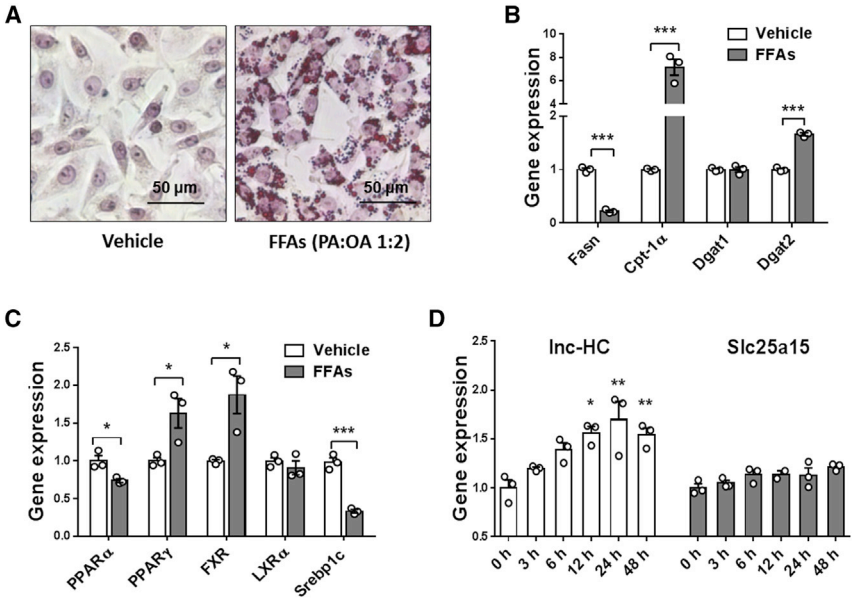

Figure 1. *lnc-HC* Expression Is Linked to Hepatocytic Fatty Acid Metabolism in CBRH-7919 Cells

(A) Oil-red O staining of CBRH-7919 cells treated with vehicle or FFAs for 24 h. (B) Quantitative real-time PCR detection of *Fasn*, *Cpt-1α*, *Dgat1*, and *Dgat2* expression in the CBRH-7919 cell model. (C) Quantitative real-time PCR analysis of *PPARα*, *PPARγ*, *FXR*, *LXRα*, and *Srebp1c* expression in the CBRH-7919 cell model. (D) Quantitative real-time PCR analysis of *lnc-HC* and *Slc25a15* expression in the CBRH-7919 cell model overtime (0, 3, 6, 12, 24, and 48 h). Data are expressed as means ± SEM. An unpaired t test was performed to determine the statistical significance. *$p < 0.05$; **$p < 0.01$; ***$p < 0.001$, as compared with, respectively, the vehicle group, the 0 h time point, or the NC group.

In our previous study, we identified a novel lncRNA, *lnc-HC* (a lncRNA derived from hepatocytes), differentially expressed in NAFLD rat livers. *lnc-HC* directly binds the co-regulator hnRNPA2B1 and further interacts with cholesterol catabolic gene *Cyp7a1* or *Abca1* as a lncRNA-protein-mRNA complex. *lnc-HC* regulates *Cyp7a1* and *Abca1* expression through hnRNPA2B1 and, thus, modulates hepatic cholesterol catabolism.[21] Based on our previous work, we further identified the function of *lnc-HC* in controlling hepatic fatty acid and triglyceride (TG) metabolism. Our present work suggests that *lnc-HC* negatively regulates *PPARγ* expression at the post-transcriptional level through the mediator *miR-130b-3p*; the *lnc-HC*/*miR-130b-3p*/*PPARγ* pathway delicately regulates the accumulation of hepatic lipid droplet.

RESULTS

lnc-HC Participates in Hepatocytic Fatty Acid Metabolism

We first induced the lipid accumulation cell model by treating CBRH-7919 and BRL3A cells with mixed free fatty acids (FFAs; 1 mM; palmitic acid [PA], oleic acid [OA]; PA:OA, 1:2) for 24 h. Oil red O staining showed obvious formation of lipid droplets in CBRH-7919 cells (Figure 1A). Meanwhile, quantitative real-time PCR results showed the expression change of the lipid metabolic enzymes fatty acid synthase (*Fasn*; 80% decrease), carnitine palmitoyl transferase 1A (*Cpt-1α*; over 7-fold increase), and diacylglycerol O-acyltransferase 2 (*Dgat2*; 1.65-fold increase) and the expression change of the lipid MNRs PPARα (25% decrease), PPARγ (1.8-fold increase), FXR (2.1-fold increase), and Srebp1c (70% decrease) in the lipid accumulation cell model (Figures 1B and 1C). We observed a time-course-dependent increase of *lnc-HC* with FFA treatment, while its overlapping gene *Slc25a15* remained unchanged (Figure 1D). Within the FFA-treated BRL3A cells, we observed the similar results as lipid droplet accumulation (Figure S1A), FFA metabolism-associated gene changes (Figures S1B and S1C), and *lnc-HC* upregulation (Figure S1D). This phenomenon suggests that *lnc-HC* takes part in hepatic FFA and TG metabolism.

lnc-HC Negatively Regulates MNR PPARγ

To figure out whether *lnc-HC* interacts with MNRs and its potential role in hepatocytic FFAs and TG metabolism, we analyzed the expression of MNRs in *lnc-HC* overexpressed and stable-knockdown cell lines, respectively named $^{overLnc\text{-}HC}$CBRH and $^{Lnc\text{-}HCshR}$CBRH. In $^{overLnc\text{-}HC}$CBRH cells, mRNA expression of *PPARγ* and *LXRα* was significantly decreased (Figure 2A). In $^{Lnc\text{-}HCshR}$CBRH cells, only *PPARγ* mRNA was increased (Figure 2B). Western blotting analysis showed consistent results that *lnc-HC* could negatively regulate PPARγ protein expression (Figure 2C). Also, *lnc-HC* negatively regulated *PPARγ* expression both at the mRNA and the protein levels in BRL3A cells (Figures S2A and S2B). *PPARγ* comprehensively controls the TG synthesis and storage process. Here, quantitative real-time PCR analysis showed that TG-synthesis-associated genes, including *Acc2*, *Acsl1*, and *Dgat2*, were negatively regulated by *lnc-HC* and that their expressions were consistent with *PPARγ* variation (Figure 2D). In addition, *lnc-HC* negatively regulated FFA uptake genes *Fatp-1* and *aP2* and the FFA β-oxidation gene *Cpt-1α* (Figure 2D). With the transfection of *PPARγ* small interfering RNA (siPPARγ; GenePharma, Shanghai, China) in $^{Lnc\text{-}HCshR}$CBRH cells, *PPARγ* expression was knocked down at the mRNA and protein levels (Figures 2E and 2F); meanwhile, the expression of *PPARγ* downstream genes, including *aP2*, *Acc2*, *Dgat2*, and *Fatp-1*, which were originally increased with *lnc-HC* knockdown, was decreased as compared with the negative control (NC) small interfering RNA group (siNC; GenePharma, Shanghai, China) (Figure 2G). Here, we confirmed that *lnc-HC* negatively regulated the expression of *PPARγ* and its pathway genes.

lnc-HC Controls *miR-130b-3p* Expression

The half-life of *PPARγ* mRNA was measured in *lnc-HC* interfered stable cell lines by the treatment of α-amanitin over 24 h to block RNA transcription by RNA polymerase II, using 18S rRNA as the normalizer control. Overexpression of *lnc-HC* reduced the half-life of the *PPARγ* transcript, while *lnc-HC* knockdown prolonged the half-life of the *PPARγ* transcript (Figure 3A). These results showed that *lnc-HC* negatively regulated *PPARγ* expression at the

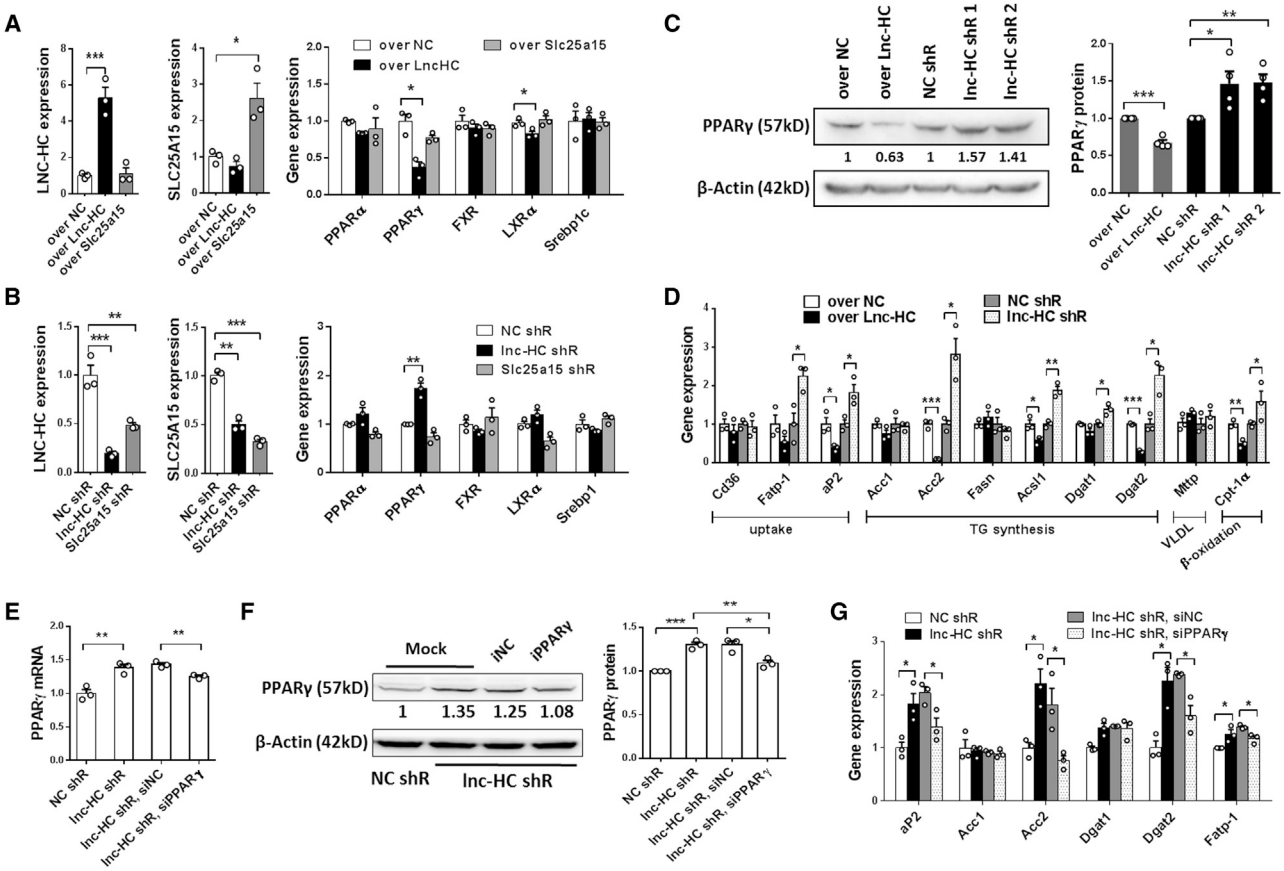

Figure 2. *lnc-HC* Controls *PPARγ* Expression and Its Signaling Pathway

(A and B) Quantitative real-time PCR analysis of gene expression, including *lnc-HC*, *Slc25a15*, *PPARα*, *PPARγ*, *FXR*, *LXRα*, and *Srebp1*, in *lnc-HC* stably overexpressed CBRH-7919 (A) and *lnc-HC* stable-knockdown CBRH-7919 cells (B). (C) Western blotting detection of *PPARγ* expression (left) and quantification histograms (right) in *lnc-HC*-overexpressed/stable-knockdown CBRH-7919. β-Actin was the loading control in the western blotting assay. Western blotting shows one representative result and quantitative data from 4 independent experiments. (D) Quantitative real-time PCR analysis of *PPARγ* target gene expressions in indicated cells. (E and F) Quantitative real-time PCR (E) and Western blotting detection (F) of *PPARγ* expression in *lnc-HC* stable-knockdown cells with siNC or siPPARγ transfection for 24 h. β-Actin was the loading control in the western blotting assay. Each western blot shows one representative result and quantitative data from three independent experiments. (G) Quantitative real-time PCR analysis of *PPARγ* target gene expression in *lnc-HC* stable-knockdown cells with siNC or siPPARγ transfection for 24 h. Data are expressed as means ± SEM. *$p < 0.05$; **$p < 0.01$; ***$p < 0.001$. An unpaired t test was performed to determine the statistical significance.

post-transcriptional level. As previously reported, *lnc-HC* regulates cholesterol catabolic genes *Cyp7a1* and *Abca1* through direct interaction with hnRNPA2B1 protein. In this study, RNA immunoprecipitation (RIP) with hnRNPA2B1 protein showed that hnRNPA2B1 could not bind the *PPARγ* transcript (Figure 3B). An RNA pulldown assay also doubly confirmed that, after the combination of *lnc-HC* and nucleoprotein (NP), there was no *PPARγ* transcript binding with the *lnc-HC*-NP complex (Figure 3C). In the RNA pulldown and hnRNPA2B1 RIP assay, *Cyp7a1* was used as positive control, which has been verified to directly interact with hnRNPA2B1. To validate the direct interaction between *lnc-HC* and the *PPARγ* transcript, we performed a GFP-RIP assay following quantitative real-time PCR. The result indicates that *lnc-HC* could not enrich the *PPARγ* transcript, using immunoglobulin G (IgG) as NC and input as loading control (Figure 3D).

As we know, microRNAs (miRNAs) modulate gene expression at the post-transcriptional level. We used miRanda and TargetScan software to predict miRNA candidates regulating *PPARγ* expression, and predicted miRNAs include *miR-130a-3p*, *miR-130b-3p*, *miR-301a-3p*, and *miR-301b-3p* (Figure 3E). To confirm whether *lnc-HC* controls expression of these candidates, we conducted quantitative real-time PCR in *lnc-HC*-interfered CBRH-7919 and BRL3A cell lines. Results displayed that only *miR-130b-3p* expression was significantly increased with *lnc-HC* overexpression and decreased with *lnc-HC* knockdown (Figures 3F and S3A). Further, we checked the expression of primary (pri-), precursor (pre-), and mature *miR-130b-3p* in *lnc-HC* knockdown and NC control cell lines. With *lnc-HC* knockdown, *pri-miR-130b* was decreased (23% decrease), *pre-miR-130b* was expressed to a lower level (50% decrease), and *miR-130b-3p* was 42% decreased (Figure 3G), which suggests that *miR-130b-3p* is regulated

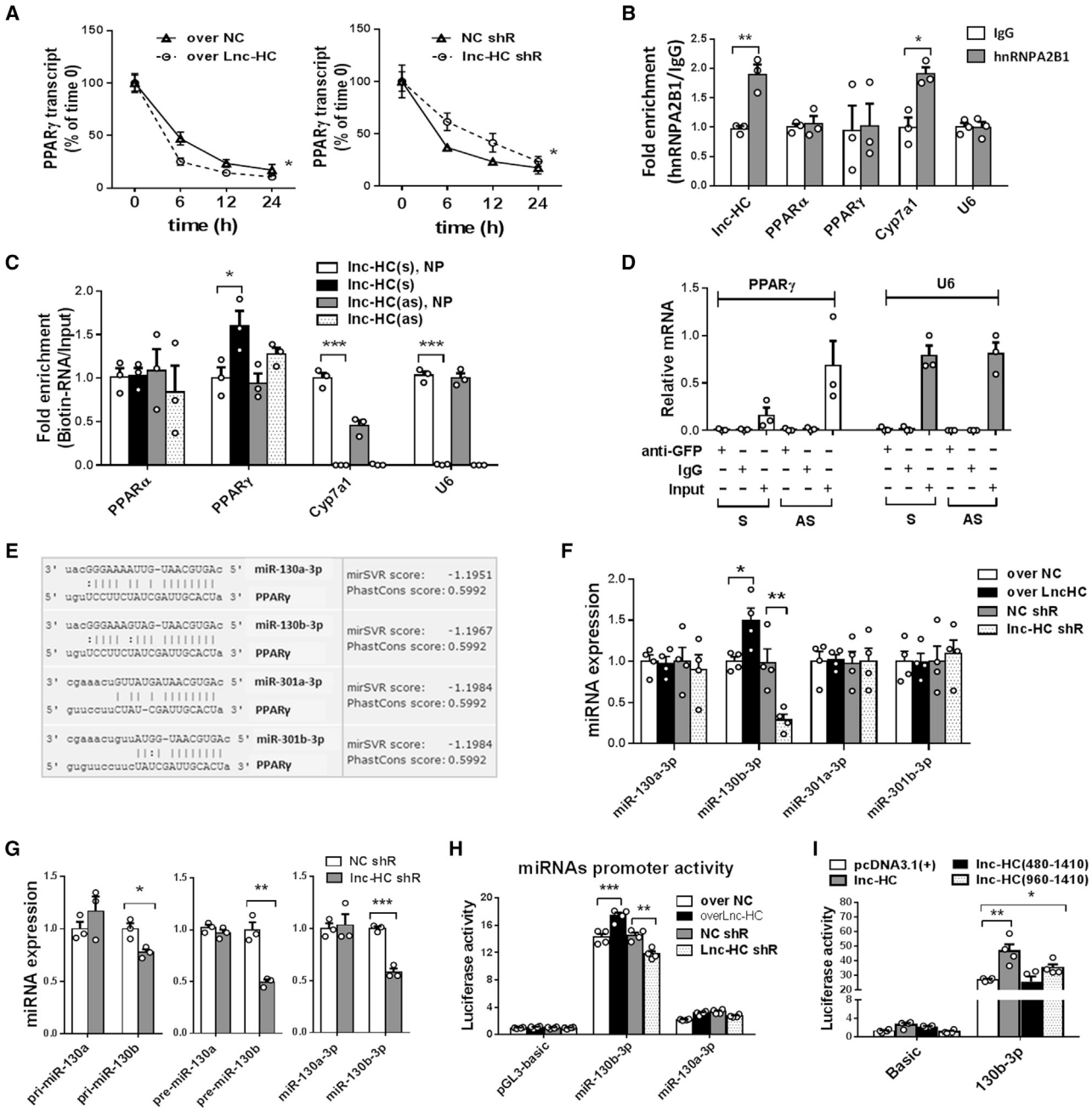

Figure 3. *lnc-HC* Modulates *miR-130b-3p* Expression

(A) Quantitative real-time PCR analysis of *PPARγ* mRNA stability overtime (0, 6, 12, and 24 h) after α-amanitin treatment (50 μM) in *lnc-HC* stably overexpressed/knockdown cells. Data are expressed as means ± SEM. *p < 0.05, NC shR versus lnc-HC shR, two-way ANOVA. (B) RIP detection of the interaction between hnRNPA2B1 protein and *lnc-HC* or indicated mRNAs, including *PPARα*, *PPARγ*, *Cyp7a1*, and *U6*, by using anti-hnRNPA2B1 antibody (5 μg), with IgG (5 μg) used as antibody isotype control. (C) RNA pull-down assay to check the interaction among *lnc-HC*, nucleoprotein (NP), and indicated mRNAs, including *PPARα*, *PPARγ*, *Cyp7a1*, and *U6*. (D) RIP detection of the interaction between *lnc-HC* and mRNAs, including *PPARγ* and *U6*, by using anti-GFP antibody (5 μg), using IgG (5 μg) as the antibody isotype control and *lnc-HC* antisense (AS) as the negative control. (E) Bioinformatics prediction results of the candidate miRNAs targeting *PPARγ* 3′UTR and the binding sequence by using miRanda and TargetScan software. (F) Quantitative real-time PCR analysis of indicated miRNA expression in *lnc-HC* stably interfered CBRH-7919. (G) Quantitative real-time PCR analysis

(legend continued on next page)

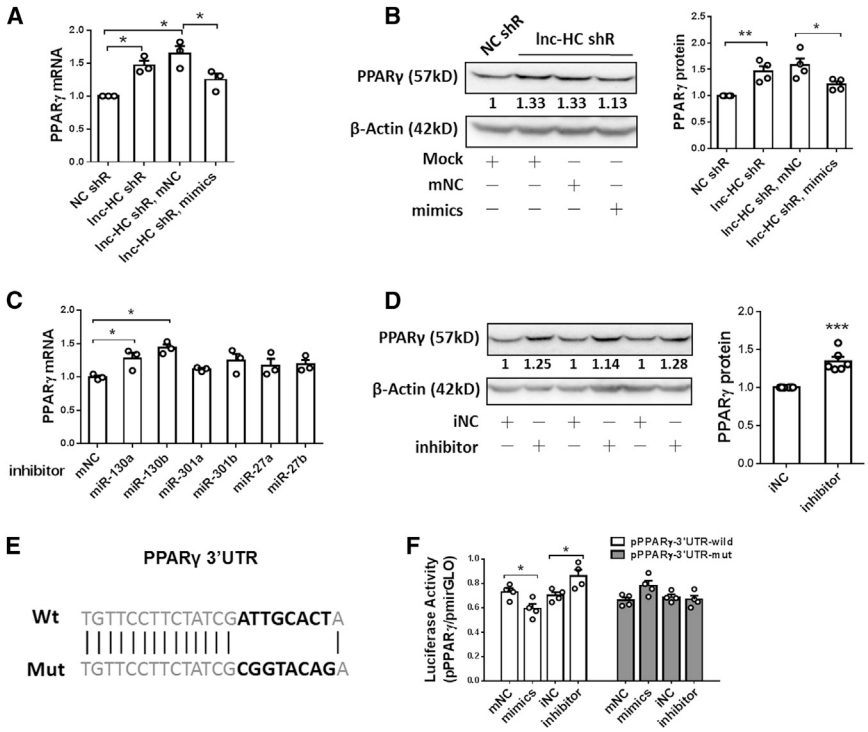

Figure 4. *lnc-HC* Controls *PPARγ* Expression through *miR-130b-3p*

(A) Quantitative real-time PCR analysis of *PPARγ* expression in *lnc-HC* stably interfered CBRH-7919, with transient transfection of NC mimics (mNC, 50 nM) or *miR-130b-3p* mimics (50 nM). (B) Western blotting measurement (left panel) and quantification histograms (right panel) of *PPARγ* expression under the same conditions as in (A). Quantitative data are from 4 independent experiments. (C) Quantitative real-time PCR analysis of *PPARγ* expression with transfection of NC inhibitor (iNC, 100 nM) or indicated miRNA inhibitors (100 nM). (D) Western blotting detection (left panel) of *PPARγ* expression in CBRH-7919 cells with transfection of iNC (100 nM) or *miR-130b-3p* inhibitor (100 nM) and quantification histograms (right panel). Western blotting and quantitative data are from 6 independent experiments. (E) Schematic diagram of wild-type (Wt) and mutated (Mut) binding sites of *miR-130b-3p* targeting *PPARγ* 3′ UTR. (F) Dual-luciferase activity of PPARγ-3′UTR-wild and PPARγ-3′UTR-mut in CBRH-7919 cells with transfection of mNC/*miR-130b-3p* mimics (50 nM) or iNC/*miR-130b-3p* inhibitor (100 nM). Data are expressed as means ± SEM. *p < 0.05; **p < 0.01; ***p < 0.001. An unpaired t test was performed to determine the statistical significance.

by *lnc-HC* from the transcriptional level to the post-transcriptional level. Subsequently, we constructed a reporter gene vector of the *miR-130b-3p* promoter region as the pGL3-130b-3p-promoter and conducted a dual-luciferase reporter assay. Results showed that *miR-130b-3p* promoter activity increased with *lnc-HC* overexpression and decreased with *lnc-HC* knockdown (Figures 3H and S3B). As previously described, the second structure of *lnc-HC* contains a 5′ stem-loop, a central stem-loop, and a 3′ stem-loop.[21] Here, a dual-luciferase reporter gene assay confirmed that the 5′ stem-loop (1–480 bp) of *lnc-HC* is critical for controlling *miR-130b-3p* promoter activity (Figures 3I and S3C).

miR-130b-3p Modulates *PPARγ* Expression

miR-130b-3p mimics and inhibitor (GenePharma, Shanghai, China) were used to check the regulation between *miR-130b-3p* and *PPARγ* expression. Mimics significantly reduced the *PPARγ* mRNA level in CBRH-7919 cells, which was originally upregulated by *lnc-HC* knockdown (Figure 4A). Consistent with the mRNA change, *miR-130b-3p* mimics also decreased PPARγ protein expression (Figure 4B). On the contrary, *PPARγ* was increased in CBRH-7919 cells after the treatment of *miR-130b-3p* inhibitor, at both the mRNA and protein levels (Figures 4C and 4D). Similarly, *miR-130b-3p* mimics strongly suppressed *PPARγ* expression, and *miR-130b-3p* inhibitor stabilized *PPARγ* expression in BRL3A cells (Figures S4A and S4B). We further constructed the reporter gene vectors pPPARγ-3′UTR-wild and pPPARγ-3′UTR-mut (Figure 4E). After transient co-transfection of CBRH-7919 cells with *miR-130b-3p* mimics/mNC (NC mimic) or *miR-130b-3p* inhibitor/iNC (NC inhibitor) and reporter gene vector pPPARγ-3′UTR-wild/mut, cells were collected to perform a dual-luciferase reporter gene assay. In the pPPARγ-3′UTR-wild transfection group, the relative luciferase activity was decreased with *miR-130b-3p* mimic treatment, while it was increased with inhibitor treatment. In addition, these changes were faded in the pPPARγ-3′UTR-mut transfection group (Figure 4F). Thus, we demonstrated that *miR-130b-3p* decreases *PPARγ* expression through binding the *PPARγ* 3′ UTR. Combined with evidence that *lnc-HC* positively regulates *miR-130b-3p* expression, it is indicated that lnc-HC controls *PPARγ* expression through the post-transcriptional modulator *miR-130b-3p*.

lnc-HC/*miR-130b-3p*/*PPARγ* Regulates Hepatocytic Lipid Metabolism

After clarifying the negative regulation of *lnc-HC* on *PPARγ* expression, we further examined the effect of *lnc-HC* on hepatocytic lipid accumulation. Oil red O staining results showed that *lnc-HC* knockdown could increase the content of cellular lipid droplets after FFA treatment as compared with the group receiving NCshR (NC shRNA [short hairpin RNA]) transfection plus FFA treatment (Figures 5A

of the expression of pri-, pre-, and mature transcripts of *miR-130a-3p* and *miR-130b-3p* in *lnc-HC* stably interfered CBRH-7919. (H) Promoter activity detection of *miR-130b-3p* and *miR-130a-3p* in *lnc-HC* stably interfered CBRH-7919 cells by using dual-luciferase reporter gene assay. (I) Dual-luciferase reporter gene assay of *miR-130b-3p* promoter activity in *lnc-HC* truncations (full-length, 480–1,410 bp, and 960–1,410 bp) transfected CBRH-7919 cells. Data are expressed as means ± SEM. *p < 0.05; **p < 0.01; ***p < 0.001. An unpaired t test was performed to determine the statistical significance.

and 5B). Consistently, the concentration of intracellular FFAs and TGs was further increased in $^{Lnc\text{-}HCshR}$CBRH cells as compared with ^{NCshR}CBRH cells (Figures 5C and 5D). It seems contradictory that *lnc-HC* expression was upregulated in hepatocytes with FFA treatment, but *lnc-HC* knockdown increased lipid accumulation. Thus, we analyzed *lnc-HC* and *PPARγ* expression in lnc-HC stably interfered cells with vehicle and FFA treatment. Quantitative real-time PCR results showed that *PPARγ* was upregulated with FFA treatment, while its increase was much higher with the decrease of *lnc-HC* in $^{lnc\text{-}HCshR}$CBRH-7919 cells; and *miR-130b-3p* expression was consistent with *lnc-HC* (Figure 5E). These results suggest that excessive FFA treatment increases *lnc-HC* and *PPARγ* expression; without lnc-HC upregulation, *PPARγ* could increase to a higher level and lead to excessive accumulation of lipid droplets in hepatocytes.

Next, we verified the effect of the *lnc-HC/miR-130b-3p/PPARγ* pathway on hepatocytic lipid accumulation. We respectively transfected $^{overLnc\text{-}HC}$CBRH cells with *miR-130b-3p* inhibitor and transfected $^{Lnc\text{-}HCshR}$CBRH cells with *miR-130b-3p* mimics for 24 h and then treated cells with FFAs for 12 h. Oil red O staining showed that lipid droplet content was reduced with *lnc-HC* overexpression, while it increased with the transfection of *miR-130b-3p* inhibitor in $^{overLnc\text{-}HC}$CBRH cells (Figures 5F and 5G). On the contrary, hepatocytic lipid accumulation was clearly increased with *lnc-HC* knockdown, while it decreased with the treatment of miR-130b-3p mimics in the $^{lnc\text{-}HCshR}$CBRH cell line (Figures 5H and 5I). These results strongly indicated that the *lnc-HC/miR-130b-3p* pathway suppresses hepatocytic lipid accumulation *in vitro*.

The Suppression of *lnc-HC* Aggravates Hepatic Lipid Disorder

Next, we checked the *in vivo* effect of *lnc-HC* in hepatic lipid metabolism. Previously, E3 rats were treated with a high-fat, high-cholesterol diet (HCD; 10% fat, 4% cholesterol and 2% sodium cholate) for 8 weeks to induce a hepatic lipid disorder condition.[21] H&E staining results showed that there was no macroscopic lipid droplet accumulation in the livers of the HCD and the HCD-plus-NCshR groups, but visible hepatic steatosis was already developed in the HCD-plus-lnc-HCshR group (Figure 6A). Serum lipid profiles were changed, TG and low-density lipoprotein-cholesterol (LDL-C) were significantly increased in the HCD group, and high-density lipoprotein-cholesterol (HDL-C) was decreased in the HCD group as compared with the control group; *lnc-HC* knockdown by using shRNA could improve serum parameters such as TG and HDL-C, but no effect was evident on serum LDL-C (Figure 6B). In addition, compared with the control group, the other three groups all showed higher liver/body weight ratios and significant increase of body weight gain (Figures 6C and 6D). Here, we focused on the hepatic metabolism changes with the variation of *lnc-HC* expression. TG concentration in rat livers was significantly increased in the HCD group as compared with the control group while further increased with *lnc-HC* knockdown by intravenous (i.v.) injection of *lnc-HC* shRNA into the HCD rat model as compared with the NC shR-plus-HCD group (Figure 6E). Meanwhile, we also checked the important gene expression in model livers. As previously shown, hepatic *lnc-HC* expression was increased in the HCD group and significantly suppressed to normal level in the *lnc-HC* shR-plus-HCD group (Figure 6F). *miR-130b-3p* expression was completely synchronized with *lnc-HC* (Figure 6G). In addition, *PPARγ* expression was significantly increased in the HCD group, as compared with the NC group, and its increase was higher in the *lnc-HC* shR-plus-HCD group at both the mRNA and protein levels (Figures 6H and 6I). Meanwhile, the overlapping gene *Slc25a15* of *lnc-HC* significantly decreased with HCD treatment *in vivo* (Figure S5). These results also verified that *lnc-HC* positively regulates *miR-130b-3p* and that the *lnc-HC/miR-130b-3p* pathway negatively controls *PPARγ* expression. Furthermore, *lnc-HC/miR-130b-3p/PPARγ* delicately modulates hepatocytic lipid accumulation and might be a therapeutic target of NAFLD.

DISCUSSION

Aberrant lipogenesis and excessive accumulation of lipid droplets in liver indicate the pathogenesis of lipid metabolism disorders and NAFLD and is closely associated with diabetes, obesity, and atherosclerosis. However, the regulatory mechanism that controls hepatic lipogenesis remains uncertain. An approved therapeutic regime is lacking due to the complexity of NAFLD pathogenesis. Some existing studies have suggested that lncRNAs are emerging as an important modulator in almost all the biological processes, which includes hepatic lipid metabolism.[22–27] In this study, we first identified *PPARγ* as the most prominent target of *lnc-HC* in hepatocytic lipid metabolism. Further study elucidates that *lnc-HC* plays a repressive role in hepatic lipid accumulation.

By quantitative real-time PCR measurement of lipid MNR expression in *lnc-HC* overexpression and knockdown cells, *PPARγ* was identified as the most prominent target of *lnc-HC* in hepatocytic lipid metabolism. Both *in vivo* and *in vitro* results elucidate that *lnc-HC* negatively regulates *PPARγ* expression through *miR-130b-3p*. Mechanically, there have been three critical regulatory patterns for lncRNAs in regulating gene expression. First, lncRNA directly interacts with specific protein as an lncRNA-protein complex, and they cooperatively control target gene expression.[28,29] Second, lncRNAs directly bind target mRNA and regulate mRNA stability.[30] Third, lncRNA and mRNA share the same recognition elements of miRNAs and increase the complexity of the miRNA regulation network, named the competitive endogenous pattern (ceRNA).[31,32] We have reported that *lnc-HC* reduces the mRNA stability of *Cyp7a1* and *Abca1* through directly interacting with the co-regulator hnRNPA2B1.[21] Here, however, we have verified that *lnc-HC* regulates *PPARγ* does not through *lnc-HC*-protein or *lnc-HC*-mRNA patterns after RNA pulldown and RIP assay. In turn, *lnc-HC* regulates *PPARγ* expression through *miR-130b-3p*, which is different from the three classical regulation patterns described earlier. *lnc-HC* controlling *miR-130b-3p* expression is involved in the level of transcription as well as the processing of miRNA precursors. As we known, the upstream signal regulation of miRNA expression is complicated. Further studies need to be done to figure out the detailed regulation between *lnc-HC* and *miR-130b-3p*, which will help us understand not only the lncRNAs' function but also miRNAs processing.

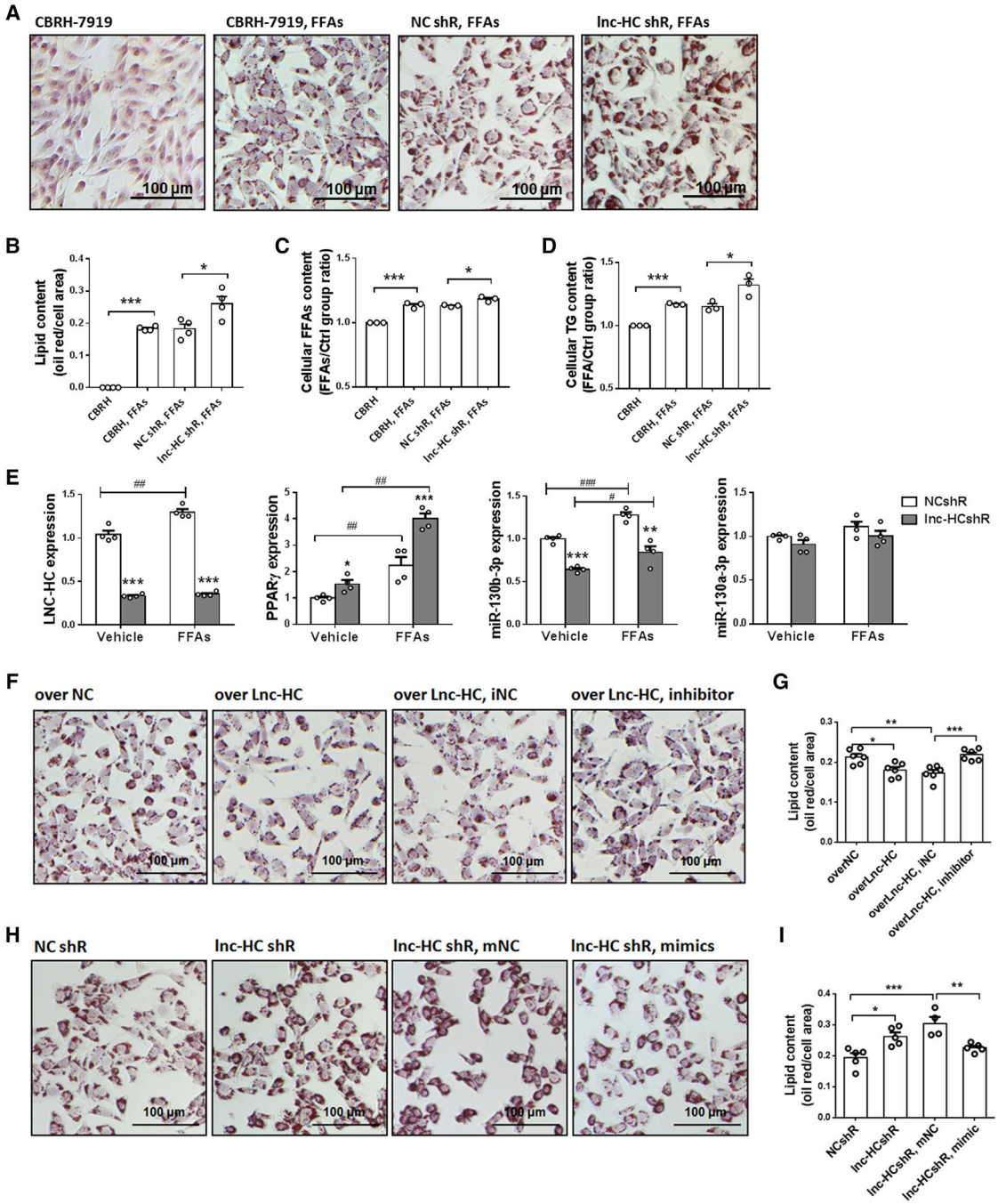

Figure 5. *lnc-HC* Negatively Regulates Hepatocytic Lipid Accumulation

(A and B) CBRH-7919, ^{NCshR}CBRH, and $^{Lnc\text{-}HCshR}$CBRH cells were treated with FFAs for 12 h, and the cellular lipid droplets in each group were (A) analyzed by oil red O staining and (B) measured by color density scanning using ImageJ. (C and D) The concentration of (C) intracellular FFAs and (D) TGs were detected. (E) Quantitative real-time PCR analysis of *lnc-HC*, *PPARγ*, and indicated miRNA expression in *lnc-HC* stably knocked down cells with vehicle or FFA treatment for 12 h. (F) $^{overLnc\text{-}HC}$CBRH cells were transfected with NC inhibitor (iNC, 100 nM) or *miR-130b-3p* inhibitor (100 nM) for 24 h and then treated with FFAs for 12 h. Oil red O staining was used to detect the lipid droplet formation in each group. (G) Quantification histograms of the relative lipid droplet content in the indicated cells by using ImageJ. (H) The lipid droplet formation was measured in $^{Lnc\text{-}HCshR}$CBRH cells under the transfection with NC mimics (mNC, 50 nM) or miR-130b-3p mimics (50 nM) for 24 h and then treated with FFAs for 12 h. (I) Quantification histograms of the relative lipid droplet content in indicated cells. Data are expressed as means ± SEM. $^{*}p < 0.05$; $^{**}p < 0.01$; $^{***}p < 0.001$, as compared, respectively, with the NC group. $^{\#}p < 0.05$; $^{\#\#}p < 0.01$; $^{\#\#\#}p < 0.001$. An unpaired t test was performed to determine the statistical significance.

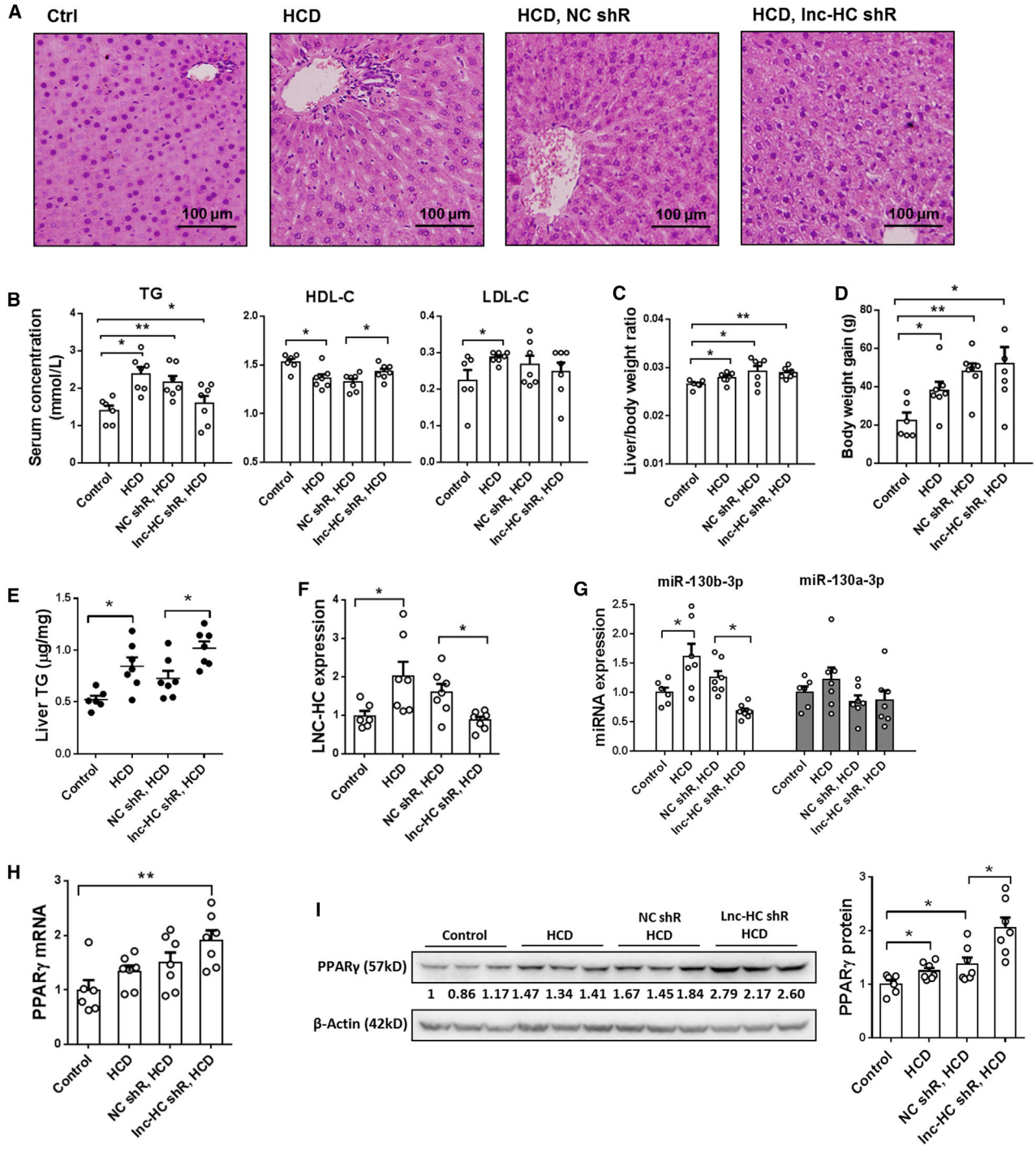

Figure 6. *lnc-HC*/*miR-130b-3p* Pathway Regulates Liver Lipid Metabolism

(A) H&E-stained liver sections with the HCD-induced lipid metabolism disorder E3 rat model. (B) At the end of the HCD-induced hyperlipidemia model (E3 rats, 8-week induction), serum concentrations of TG, HDL-C, and LDL-C were measured. (C and D) The liver/body weight ratio (C) and body weight gain (D) at the 8th week. (E) The hepatic TG concentration. (F and G) Quantitative real-time PCR analysis of *lnc-HC* expression (F) and *miR-130b-3p* and *miR-130a-3p* expression (G) in rat livers. (H and I) Quantitative real-time PCR analysis (H) and western blotting detection (I) of *PPARγ* expression in model livers. Data are expressed as means ± SEM. *$p < 0.05$; **$p < 0.01$; ***$p < 0.001$. An unpaired t test was performed to determine the statistical significance.

Our previous findings declared that *lnc-HC* negatively regulates hepatic cholesterol catabolism. In an 8-week high-fat HCD-induced hepatic lipid disorder model, serum concentrations of TG and HDL-C were significantly improved with *lnc-HC* suppression, which indicates a therapy potential of *lnc-HC* knockdown in body lipid metabolism disorder. Regarding model liver, *lnc-HC* suppression significantly increased TG concentration and vacuolar-like steatosis phenotype. These parameters point out the multifunction of *lnc-HC* in systemic lipid metabolism as a good effect in dyslipidemia but as side effects in hepatic lipid metabolism. *In vitro*, the knockdown of *lnc-HC* significantly upregulates FFA uptake genes *Fatp-1* and *aP2* and TG synthesis genes *Acc2, Acsl1*, and *Dgat2*, while it has little effect on hepatocytic very low-density lipoprotein (VLDL) formation genes *Dgat1* and *Mttp*. *In vivo*, *lnc-HC* has little effect on serum LDL-C concentration, which is derived most partly from TG-enriched VLDL-C. These results could explain the hepatic TG increase and serum TG decrease. *lnc-HC* also negatively regulates mitochondrial FFA β-oxidation gene *Cpt-1α*, suggesting that its potential role in FFA consumption and utilization needs to be studied. Combined with the lipid accumulation test, we found that the comprehensive effect of *lnc-HC* is promoting FFA uptake, TG synthesis, and lipid droplet accumulation in cells. *In vivo* experiments showed that *lnc-HC* knockdown could aggregate lipid metabolism disorder in rat liver as vacuolar-like hepatic steatosis, which strongly indicates the protective role of *lnc-HC* in liver from excessive lipid droplet accumulation.

The exact signal that triggers *lnc-HC* expression is not measured in this study, but our previous work has reported that LXR agonist T0901317 could induce *lnc-HC*.[21] Thus, LXRs might provide an upstream signal that drives hepatic lipogenesis and *lnc-HC* overexpression. Here, *lnc-HC* represses hepatocytic lipid droplet accumulation through negative regulation of *PPARγ* expression. It seems contradictory that FFA induces *lnc-HC* expression in CBRH-7919 and BRL3A cells, but *lnc-HC* overexpression suppresses hepatocytic lipid droplet formation, and knockdown *lnc-HC* expression increases hepatocytic lipid accumulation and liver TG concentration. Focused on this question, our quantitative real-time PCR results showed that *PPARγ* was upregulated in FFA-treated cells and HCD-treated rat livers, while it increased much higher with the decrease of *lnc-HC*, and that *miR-130b-3p* expression was consistent with *lnc-HC*. Hence, it is suggested that *PPARγ* could be upregulated much higher and lead to hepatocytic lipid overaccumulation without *lnc-HC* upregulation. This delicate modulation is consistent with the fine-tuning regulation pattern of lncRNAs and miRNAs. Here, our findings support a protection role of *lnc-HC* in preventing excessive lipogenesis, lipid accumulation, and NAFLD phenotype within the liver.

Taken together, we further identify the function and molecular mechanism of *lnc-HC* in inhibiting the accumulation of lipid droplets in liver through negatively regulating *PPARγ* expression. Under FFA treatment, the upregulated *lnc-HC* protects hepatocytes from excessively overexpressing *PPARγ* and helps avoid excessive formation of lipid droplets and lipid accumulation in liver. *lnc-HC* contributes hepatic lipid homeostasis through a versatile and complex mechanism, and these results may supply more detailed and integrated information to open new therapeutic strategies for the prevention and treatment of NAFLD.

MATERIALS AND METHODS

Animals

The animal experiments were approved by the Institutional Animal Ethics Committee of Xi'an Jiaotong University School of Medicine (permission ID: XJ2006Y039; Xi'an Jiaotong University, Xi'an, China), and were performed in accordance with the European Communities Council Directive 2010/63/EU for the protection of animals used for scientific purposes.

E3 rats originated from Lund University (Lund, Sweden) and were maintained in 12-h/12-h light/dark cycles under specific pathogen-free conditions. As previously described,[21] 27 E3 rats (8–12 weeks old) were randomly divided into 4 groups, including a control group (n = 6), a high-fat HCD group (n = 7), an HCD and NC shRNA i.v. injection group (HCD, NCshR; n = 7), and an HCD and lnc-HC shRNA i.v. injection group (HCD, lnc-HCshR; n = 7). After being fed for 8 weeks with a normal diet or an HCD diet (10% fat, 4% cholesterol, and 2% sodium cholate), rats were euthanized by intraperitoneal (i.p.) injection of pentobarbital sodium (30 mg/kg) for blood collection, liver collection, and subsequent measurements.

Cell Culture

CBRH-7919 cells were maintained in RPMI-1640 medium (Hyclone Laboratories, South Logan, UT, USA) containing 10% FBS (GIBCO, Gaithersburg, MD, USA). BRL3A cells were maintained in DMEM (GIBCO, Gaithersburg, MD, USA) containing 10% FBS (GIBCO, Gaithersburg, MD, USA). For lipid droplet formation and oil red O staining, CBRH-7919 cells and BRL3A cells were plated in a 12-well plate. After 24 h, cells were treated with mixed FFAs (1 mM; PA:OA, 1:2 in RPMI-1640 medium containing 2% FBS) for the indicated time. Then, oil red O staining was conducted to determine the cellular lipid droplet formation. Treated cells were visualized using microscopy (Olympus, Tokyo, Japan). TG and FFA levels of cells and rat livers were measured, respectively, by using the Total Triglyceride Assay Kit (Nanjing Jiancheng, Nanjing, China) or the Non-esterified Free Fatty Acids Assay Kit (Nanjing Jiancheng, Nanjing, China), following the manufacturer's instructions.

lnc-HC and *Slc25a15* Gene Overexpression and Knockdown

Expression vector construction was as previously reported.[21] Briefly, *lnc-HC* DNA was obtained by PCR with PrimeSTAR GXL DNA Polymerase (Takara Bio, Beijing, China) and inserted into the pcDNA3.1(+) vector between *Hin*d III and *Eco*R I sites, named pcDNA3.1-lnc-HC. The *Slc25a15* coding region was obtained by PCR and inserted into the pcDNA3.1(+) vector between *Bam*H I and *Xho* I, named pcDNA3.1-Slc25a15. Information on the primers is depicted in Table S1. The shRNAs for *lnc-HC* or *Slc25a15* gene knockdown were ordered and synthesized by GenePharma.[31] The target sequences for *lnc-HC* and *Slc25a15* gene knockdown assay are depicted in Table S2. After a 24-h transfection

of these recombinant plasmids in CBRH-7919 cells by using Lipofectamine 2000 (Invitrogen, Waltham, MA, USA) according to the manufacturer's instructions, G418 was added into cell culture medium at 500 μg/mL to select the monoclonal stable cell lines respectively named $^{overLnc\text{-}HC}$CBRH, ^{overSlc25a15}CBRH, ^{NCshR}CBRH, and $^{Lnc\text{-}HCshR}$CBRH. In *lnc-HC* interfered stable cells, small interfering RNAs (siRNAs) of PPARγ were used to check the regulation of *lnc-HC* on the *PPARγ* signaling pathway. The sequence information of *PPARγ* siRNAs is depicted in Table S2. In BRL3A cells, recombinant plasmids were transfected into cells by using Lipofectamine 2000 (Invitrogen, Waltham, MA, USA) for 24 h for RNA isolation and 48 h for protein isolation.

RNA Isolation, Reverse Transcription, and Quantitative Real-Time PCR

RNA from cells or rat liver tissues was extracted by using TRIzol Reagent (Invitrogen, Waltham, MA, USA). RNA concentration and quality were detected by NanoDrop. cDNAs for mRNA expression detection were reverse transcribed with 5 μg total RNA per sample by using the RevertAid First Strand cDNA Synthesis Kit (Thermo Fisher Scientific, Waltham, MA, USA), and miRNA cDNAs were transcribed with 2 μg total RNA per sample by using the Mir-X miRNA qRT-PCR SYBR Kit (Clontech Laboratories, Mountain View, CA, USA). Quantitative real-time PCR was performed by using the SYBR Green qPCR Master Mix (Clontech, Mountain View, CA, USA) in the Agilent Mx3005P and Bio-Rad iQ5 systems. The detection program of gene expression with cDNA transcribed from mRNA is: 10 min at 95°C, 40 cycles of 10 s at 95°C, 10 s at annealing temperature, and 30 s at 72°C. The program of miRNA cDNA detection is: 10 min at 95°C, 40 cycles of 10 s at 95°C, and 30 s at 60°C. Melting curves were performed to check quantitative real-time PCR products. Data were normalized by *β-actin* for mRNA expression and by *U6* for miRNAs. The gene primer information for quantitative real-time PCR is depicted in Table S3. miRNA primer information for quantitative real-time PCR is depicted in Table S4.

Western Blotting

Protein was isolated from cells and rat model livers by using cell lysis buffer (Beyotime Biotechnology, Shanghai, China). Protein samples were separated by 10% SDS-PAGE gel and transferred onto polyvinylidene fluoride (PVDF) membranes (Bio-Rad, Hercules, CA, USA) according to the standard process. Gene expression at the protein level was detected by using rabbit anti-PPARγ antibody (Abcam, Cambridge, MA, USA; 1:1,000), rabbit anti-Slc25a15 antibody (Abcam, Cambridge, MA, USA; 1:1,000) or rabbit anti-β-actin antibody (Santa Cruz Biotechnology, Shanghai, China; 1:500).

RNA Immunoprecipitation

For detecting the interaction between hnRNPA2B1 and candidate RNAs, RIP was performed as previously described.[21,28,33] Briefly, the cell nucleus was obtained by using the Nuclear and Cytoplasmic Protein Extraction Kit (Beyotime Biotechnology, Shanghai, China). Nuclear extract was lysed with polysome lysis buffer (100 mM KCl, 5 mM $MgCl_2$, 10 mM HEPES [pH 7.0], 0.5% NP-40, and 1 mM DTT, with added cOmplete protease inhibitors [Roche, Basel, Switzerland] and RNase inhibitor [Ambion, Austin, TX, USA] before use). Rabbit anti-hnRNPA2B1 antibody (Abcam, Cambridge, UK) or rabbit isotype IgG per 5 μg was used in each respective RIP reaction. Binding RNAs were isolated by phenol-chloroform-isoamyl alcohol for quantitative real-time PCR assay.

To detect the direct interaction between *lnc-HC* and candidate mRNAs, we constructed recombinant plasmids first. The *lnc-HC* DNA was obtained by PCR with PrimeSTAR GXL DNA Polymerase (Takara Bio, Beijing, China) and inserted forward or reversely into pcDNA3.1(+) vector between *Hin*d III and *Eco*R I sites, respectively named pcDNA3.1-lnc-HC(sense) and pcDNA3.1-lnc-HC(antisense). Then, pSL-MS2-12X (Addgene, USA), pcDNA3.1-lnc-HC(sense), and pcDNA3.1-lnc-HC(antisense) were double digested with *Eco*R I and *Xho* I. The MS2-12X fragment, the digestion product of pSL-MS2-12X, was inserted into pcDNA3.1-lnc-HC(sense) or pcDNA3.1-lnc-HC(antisense), respectively named pcDNA3.1-MS2-lnc-HC(sense) and pcDNA3.1-MS2-lnc-HC(antisense). These vectors were used to determine the interaction between *lnc-HC* and candidate mRNAs by RIP assay. CBRH-7919 cells were co-transfected with pMS2-GFP (Addgene, Watertown, MA, USA) and pcDNA3.1-MS2-lnc-HC(sense) or pcDNA3.1-MS2-lnc-HC(antisense). After 48 h of transfection, cells were harvested to perform a RIP assay by using the Magna RIP RNA-Binding Protein Immunoprecipitation Kit (Millipore, Cleveland, OH, USA) according to the manufacturer's instructions. Rabbit anti-GFP antibody (Abcam, Cambridge, UK) or rabbit isotype IgG (Beyotime Biotechnology, Shanghai, China) per 5 μg were used in each respective RIP reaction system.[34]

RNA Pulldown

For detecting the interaction among *lnc-HC*, nucleus protein, and target mRNAs, RNA pulldown was performed by using the Pierce Magnetic RNA-Protein Pull-Down Kit (Pierce, Waltham, MA, USA). Briefly, biotin-labeled RNAs were transcribed *in vitro* by using Biotin RNA Labeling Mix (Roche, Basel, Switzerland) and T7 RNA polymerase (Ambion, Austin, TX, USA), and purified by phenol-chloroform-isoamyl alcohol. After the binding between folded biotin-lnc-HC (sense or antisense) and nucleus protein, folded total RNA (~250 μg) of CBRH-7919 cells was added into purified beads. After incubation and bead washing, the RNA component was isolated by phenol-chloroform-isoamyl alcohol for quantitative real-time PCR assay.

Dual-Luciferase Reporter Gene Assay

The recombinant vectors of *PPARγ* 3′UTR (wild and mut) for checking interaction between miRNA candidates and *PPARγ* by dual-luciferase reporter gene assay were constructed by GeneChem (Shanghai, China) and, respectively, named pPPARγ-3′UTR-wild and pPPARγ-3′UTR-mut. The DNA fragments of *PPARγ* 3′UTR-wild and *PPARγ* 3′UTR-mut are listed in Table S1. CBRH-7919 cells were seeded into a 48-well plate. CBRH-7919 cells were co-transfected with pPPARγ-3′UTR-wild (100 ng) or pPPARγ-3′UTR-mut (100 ng) and miRNA

small molecules (100 nM), such as mNCs, miR-130b3p mimics, iNCs, or miR-130b-3p inhibitors (purchased from GenePharma, Shanghai, China) by Lipofectamine 2000 reagent (Invitrogen, Waltham, MA, USA). After 24 h of transfection, the relative luciferase activity of each group was measured using the Dual-Luciferase Reporter Assay System (Promega, Madison, WI, USA), according to the manufacturer's instructions.

The promoter regions of *miR-130b-3p* and *miR-130a-3p* were generated by PCR. The primer information is depicted in Table S1. They were cloned into pGL3-basic vectors between *Kpn*I and *Nhe* I sites named pGL3-130b-3p-promoter and pGL3-130a-3p-promoter, respectively. For detecting the promoter activity of *miR-130a-3p* and *miR-130b-3p*, pGL3-promoter/pRL (90:10 ng per well) was co-transfected into CBRH-7919 or BRL3A cells (in a 48-well plate) for 24 h. pGL3-basic/pRL (90:10 ng per well) was used as NC. Luciferase activity was measured by using the Dual-Luciferase Reporter Assay System (Promega, Madison, WI, USA), following the manufacturer's instructions.

Statistical Analysis

Quantitative data were expressed as means ± SEM. The statistical analysis of difference between groups was performed by unpaired Student's t test. A two-way ANOVA was used to analyze the differences of mRNA stability after α-amanitin treatment in indicated cell lines. $p < 0.05$ was considered statistically significant.

SUPPLEMENTAL INFORMATION

Supplemental Information can be found online at https://doi.org/10.1016/j.omtn.2019.10.018.

AUTHOR CONTRIBUTIONS

Study design: X.L. and S.L. Analysis and interpretation of data: S.L. and X.L. Drafting of the manuscript: X.L. Critical revision of the manuscript: X.L. and S.L. Obtained funding: X.L. Performance of the experiment: X.L., N.W., Q.C., and L.W. Preparation and assistant work: Yue L., X.D., C.W., L.F., Yazhao L., E.K.O., M.S., and Q.N. Necessary technical guides: D.L., X. Yan, and X. Yang.

CONFLICT OF INTERESTS

The authors declare no competing interests.

ACKNOWLEDGMENTS

The project was supported by the National Natural Science Foundation of China (81600679 to X.L. and 81770864 to D.L.), the China Postdoctoral Science Foundation (2016M592778 to X.L.), the Fundamental Research Funds for the Central Universities (xjj2017051 to X.L. and zrzd2017007 to D.L.), and the Shaanxi Postdoctoral Science Foundation (2016BSHEDZZ98 to X.L.).

REFERENCES

1. Anstee, Q.M., McPherson, S., and Day, C.P. (2011). How big a problem is non-alcoholic fatty liver disease? BMJ *343*, d3897.
2. Ahmed, A., Wong, R.J., and Harrison, S.A. (2015). Nonalcoholic fatty liver disease review: diagnosis, treatment, and outcomes. Clin. Gastroenterol. Hepatol. *13*, 2062–2070.
3. Baffy, G., Brunt, E.M., and Caldwell, S.H. (2012). Hepatocellular carcinoma in non-alcoholic fatty liver disease: an emerging menace. J. Hepatol. *56*, 1384–1391.
4. Ekstedt, M., Hagström, H., Nasr, P., Fredrikson, M., Stål, P., Kechagias, S., and Hultcrantz, R. (2015). Fibrosis stage is the strongest predictor for disease-specific mortality in NAFLD after up to 33 years of follow-up. Hepatology *61*, 1547–1554.
5. Yki-Järvinen, H. (2014). Non-alcoholic fatty liver disease as a cause and a consequence of metabolic syndrome. Lancet Diabetes Endocrinol. *2*, 901–910.
6. Torres, D.M., and Harrison, S.A. (2015). Nonalcoholic fatty liver disease: fibrosis portends a worse prognosis. Hepatology *61*, 1462–1464.
7. Ofosu, A., Ramai, D., and Reddy, M. (2018). Non-alcoholic fatty liver disease: controlling an emerging epidemic, challenges, and future directions. Ann. Gastroenterol. *31*, 288–295.
8. Anstee, Q.M., Mantovani, A., Tilg, H., and Targher, G. (2018). Risk of cardiomyopathy and cardiac arrhythmias in patients with nonalcoholic fatty liver disease. Nat. Rev. Gastroenterol. Hepatol. *15*, 425–439.
9. Arrese, M., and Karpen, S.J. (2010). Nuclear receptors, inflammation, and liver disease: insights for cholestatic and fatty liver diseases. Clin. Pharmacol. Ther. *87*, 473–478.
10. Wang, Y., Viscarra, J., Kim, S.J., and Sul, H.S. (2015). Transcriptional regulation of hepatic lipogenesis. Nat. Rev. Mol. Cell Biol. *16*, 678–689.
11. Stump, M., Mukohda, M., Hu, C., and Sigmund, C.D. (2015). PPARγ regulation in hypertension and metabolic syndrome. Curr. Hypertens. Rep. *17*, 89.
12. Larsen, T.M., Toubro, S., and Astrup, A. (2003). PPARgamma agonists in the treatment of type II diabetes: is increased fatness commensurate with long-term efficacy? Int. J. Obes. Relat. Metab. Disord. *27*, 147–161.
13. Li, Y., Qi, Y., Huang, T.H., Yamahara, J., and Roufogalis, B.D. (2008). Pomegranate flower: a unique traditional antidiabetic medicine with dual PPAR-alpha/-gamma activator properties. Diabetes Obes. Metab. *10*, 10–17.
14. Wutz, A. (2011). Gene silencing in X-chromosome inactivation: advances in understanding facultative heterochromatin formation. Nat. Rev. Genet. *12*, 542–553.
15. Lee, J.T. (2011). Gracefully ageing at 50, X-chromosome inactivation becomes a paradigm for RNA and chromatin control. Nat. Rev. Mol. Cell Biol. *12*, 815–826.
16. Wapinski, O., and Chang, H.Y. (2011). Long noncoding RNAs and human disease. Trends Cell Biol. *21*, 354–361.
17. Shi, X., Sun, M., Liu, H., Yao, Y., and Song, Y. (2013). Long non-coding RNAs: a new frontier in the study of human diseases. Cancer Lett. *339*, 159–166.
18. Divoux, A., Karastergiou, K., Xie, H., Guo, W., Perera, R.J., Fried, S.K., and Smith, S.R. (2014). Identification of a novel lncRNA in gluteal adipose tissue and evidence for its positive effect on preadipocyte differentiation. Obesity (Silver Spring) *22*, 1781–1785.
19. Zhao, X.Y., Li, S., Wang, G.X., Yu, Q., and Lin, J.D. (2014). A long noncoding RNA transcriptional regulatory circuit drives thermogenic adipocyte differentiation. Mol. Cell *55*, 372–382.
20. Li, P., Ruan, X., Yang, L., Kiesewetter, K., Zhao, Y., Luo, H., Chen, Y., Gucek, M., Zhu, J., and Cao, H. (2015). A liver-enriched long non-coding RNA, lncLSTR, regulates systemic lipid metabolism in mice. Cell Metab. *21*, 455–467.
21. Lan, X., Yan, J., Ren, J., Zhong, B., Li, J., Li, Y., Liu, L., Yi, J., Sun, Q., Yang, X., et al. (2016). A novel long noncoding RNA Lnc-HC binds hnRNPA2B1 to regulate expressions of Cyp7a1 and Abca1 in hepatocytic cholesterol metabolism. Hepatology *64*, 58–72.
22. Wang, Y., Tang, H., Ji, X., Zhang, Y., Xu, W., Yang, X., Deng, R., Liu, Y., Li, F., Wang, X., and Zhou, L. (2018). Expression profile analysis of long non-coding RNAs involved in the metformin-inhibited gluconeogenesis of primary mouse hepatocytes. Int. J. Mol. Med. *41*, 302–310.
23. Liu, C., Yang, Z., Wu, J., Zhang, L., Lee, S., Shin, D.J., Tran, M., and Wang, L. (2018). Long noncoding RNA H19 interacts with polypyrimidine tract-binding protein 1 to reprogram hepatic lipid homeostasis. Hepatology *67*, 1768–1783.

24. Wang, J., Yang, W., Chen, Z., Chen, J., Meng, Y., Feng, B., Sun, L., Dou, L., Li, J., Cui, Q., and Yang, J. (2018). Long noncoding RNA lncSHGL recruits hnRNPA1 to suppress hepatic gluconeogenesis and lipogenesis. Diabetes *67*, 581–593.

25. Guo, J., Fang, W., Sun, L., Lu, Y., Dou, L., Huang, X., Tang, W., Yu, L., and Li, J. (2018). Ultraconserved element uc.372 drives hepatic lipid accumulation by suppressing miR-195/miR4668 maturation. Nat. Commun. *9*, 612.

26. Zhang, M., Chi, X., Qu, N., and Wang, C. (2018). Long noncoding RNA lncARSR promotes hepatic lipogenesis via Akt/SREBP-1c pathway and contributes to the pathogenesis of nonalcoholic steatohepatitis. Biochem. Biophys. Res. Commun. *499*, 66–70.

27. Zhao, X.Y., Xiong, X., Liu, T., Mi, L., Peng, X., Rui, C., Guo, L., Li, S., Li, X., and Lin, J.D. (2018). Long noncoding RNA licensing of obesity-linked hepatic lipogenesis and NAFLD pathogenesis. Nat. Commun. *9*, 2986.

28. Wang, P., Xue, Y., Han, Y., Lin, L., Wu, C., Xu, S., Jiang, Z., Xu, J., Liu, Q., and Cao, X. (2014). The STAT3-binding long noncoding RNA lnc-DC controls human dendritic cell differentiation. Science *344*, 310–313.

29. Yang, F., Zhang, H., Mei, Y., and Wu, M. (2014). Reciprocal regulation of HIF-1α and lincRNA-p21 modulates the Warburg effect. Mol. Cell *53*, 88–100.

30. Greco, S., Zaccagnini, G., Fuschi, P., Voellenkle, C., Carrara, M., Sadeghi, I., Bearzi, C., Maimone, B., Castelvecchio, S., Stellos, K., et al. (2017). Increased BACE1-AS long noncoding RNA and β-amyloid levels in heart failure. Cardiovasc. Res. *113*, 453–463.

31. Cesana, M., Cacchiarelli, D., Legnini, I., Santini, T., Sthandier, O., Chinappi, M., Tramontano, A., and Bozzoni, I. (2011). A long noncoding RNA controls muscle differentiation by functioning as a competing endogenous RNA. Cell *147*, 358–369.

32. Wang, Y., Pang, W.J., Wei, N., Xiong, Y., Wu, W.J., Zhao, C.Z., Shen, Q.W., and Yang, G.S. (2014). Identification, stability and expression of Sirt1 antisense long non-coding RNA. Gene *539*, 117–124.

33. Ng, S.Y., Bogu, G.K., Soh, B.S., and Stanton, L.W. (2013). The long noncoding RNA RMST interacts with SOX2 to regulate neurogenesis. Mol. Cell *51*, 349–359.

34. Yuan, J.H., Yang, F., Wang, F., Ma, J.Z., Guo, Y.J., Tao, Q.F., Liu, F., Pan, W., Wang, T.T., Zhou, C.C., et al. (2014). A long noncoding RNA activated by TGF-β promotes the invasion-metastasis cascade in hepatocellular carcinoma. Cancer Cell *25*, 666–681.